

NASA/TM-20230013058



Electron Beam Welding of Additively Manufactured Niobium Alloy Heat Pipes

*Eric Brizes and Justin Milner
Glenn Research Center, Cleveland, Ohio*

January 2024

NASA STI Program . . . in Profile

Since its founding, NASA has been dedicated to the advancement of aeronautics and space science. The NASA Scientific and Technical Information (STI) Program plays a key part in helping NASA maintain this important role.

The NASA STI Program operates under the auspices of the Agency Chief Information Officer. It collects, organizes, provides for archiving, and disseminates NASA's STI. The NASA STI Program provides access to the NASA Technical Report Server—Registered (NTRS Reg) and NASA Technical Report Server—Public (NTRS) thus providing one of the largest collections of aeronautical and space science STI in the world. Results are published in both non-NASA channels and by NASA in the NASA STI Report Series, which includes the following report types:

- TECHNICAL PUBLICATION. Reports of completed research or a major significant phase of research that present the results of NASA programs and include extensive data or theoretical analysis. Includes compilations of significant scientific and technical data and information deemed to be of continuing reference value. NASA counter-part of peer-reviewed formal professional papers, but has less stringent limitations on manuscript length and extent of graphic presentations.
- TECHNICAL MEMORANDUM. Scientific and technical findings that are preliminary or of specialized interest, e.g., “quick-release” reports, working papers, and bibliographies that contain minimal annotation. Does not contain extensive analysis.
- CONTRACTOR REPORT. Scientific and technical findings by NASA-sponsored contractors and grantees.
- CONFERENCE PUBLICATION. Collected papers from scientific and technical conferences, symposia, seminars, or other meetings sponsored or co-sponsored by NASA.
- SPECIAL PUBLICATION. Scientific, technical, or historical information from NASA programs, projects, and missions, often concerned with subjects having substantial public interest.
- TECHNICAL TRANSLATION. English-language translations of foreign scientific and technical material pertinent to NASA's mission.

For more information about the NASA STI program, see the following:

- Access the NASA STI program home page at <http://www.sti.nasa.gov>
- E-mail your question to help@sti.nasa.gov
- Fax your question to the NASA STI Information Desk at 757-864-6500
- Telephone the NASA STI Information Desk at 757-864-9658
- Write to:
NASA STI Program
Mail Stop 148
NASA Langley Research Center
Hampton, VA 23681-2199

NASA/TM-20230013058



Electron Beam Welding of Additively Manufactured Niobium Alloy Heat Pipes

*Eric Brizes and Justin Milner
Glenn Research Center, Cleveland, Ohio*

National Aeronautics and
Space Administration

Glenn Research Center
Cleveland, Ohio 44135

January 2024

Acknowledgments

The research at NASA Glenn Research Center was funded by a NASA Center Innovation Fund (CIF) project titled “Additive Manufacturing of In-Core Heat Pipes for Space Nuclear Power and Propulsion.” The meticulous electron beam welding of Christopher Metro, consistent CT scanning and analysis of Richard Rauser and Richard Martin, and metallographic preparations of graduate fellow Carter Fietek at NASA Glenn Research Center are greatly appreciated.

Trade names and trademarks are used in this report for identification only. Their usage does not constitute an official endorsement, either expressed or implied, by the National Aeronautics and Space Administration.

Level of Review: This material has been technically reviewed by technical management.

Electron Beam Welding of Additively Manufactured Niobium Alloy Heat Pipes

Eric Brizes and Justin Milner
National Aeronautics and Space Administration
Glenn Research Center
Cleveland, Ohio 44135

Abstract

Additively manufactured (AM) refractory alloy-liquid metal heat pipes are being developed and tested for thermal management systems within nuclear propulsion and power applications. This study investigated electron beam (EB) welded joints on a laser powder bed fusion printed niobium alloy (C-103) and the impact of multiple joined heat pipe sections on working fluid flow and container leak-tightness. Results showed that EB welded joints connecting multiple heat pipe sections do not impact working fluid wicking behavior and the printed C-103 material and the EB welds joining the tubular sections created a leak-tight container. Interestingly, computed tomography (CT) data showed an order of magnitude greater number and volume of porosity indications in the ground mating surface weld compared to the as-printed mating surface weld. The work concluded that AM is a viable manufacturing process for niobium alloy heat pipes and provided valuable insights for future AM heat pipe research and development.

1.0 Introduction

High-temperature liquid metal heat pipes are being developed and tested for nuclear electric propulsion (NEP), nuclear thermal propulsion (NTP), and fission surface power (FSP) applications. Reactor designs necessitate the movement of heat from the nuclear core to power conversion systems (e.g., Stirling engine) using heat pipes (Ref. 1). Heat pipes passively transfer thermal energy using a two-phase evaporation and condensation cycle that occurs within a sealed tube lined with an internal wick structure. The wick assists capillary forces acting to return the working fluid back to the hot side of the device for completion of the thermal cycle. Refractory metals, particularly niobium, can serve as a suitable heat pipe construction materials due to their tolerance of the in-core neutron environment and compatibility with the higher-temperature liquid metal heat pipe working fluids such as sodium and lithium. Advances in additive manufacturing (AM) of refractory metals including niobium have opened the high-temperature heat pipe design space.

AM has proven to be a disruptive technology in the aerospace industry and its impact has reached heat pipe fabrication. A review of recent developments in heat pipe production via AM was performed by P. Szymanski and D. Mikielewicz in 2022 (Ref. 2). AM is touted as a solution to many challenges encountered during heat pipe production like manufacturing of complex wick structures, unusual pipe geometries, gravity friendly wicks, and easily sealable leak-free pipes. Furthermore, the density of partially sintered internal wick structures can be optimized and functionally graded throughout a single component. Studies of printed heat pipes have shown increased thermal conductivity, improved geometric sizing, cheaper overall fabrication, enhanced thermal performance against gravity, and improved reliability compared to conventionally manufactured aluminum, titanium, copper, and stainless-steel heat pipes (Ref. 2).

Recent work by D. H. Lee and I. C. Bang of UNIST in the Republic of Korea (2021) has shown progress in development of additively manufactured high-temperature liquid-metal heat pipes for nuclear

applications (Ref. 3). An axially grooved heat pipe was printed using the laser powder bed fusion (L-PBF) process and included alignment features on adjoining surfaces. In their work, the joining of multiple printed heat pipe sections was necessary because the maximum length of the L-PBF parts achievable was 30 cm due to AM equipment limitations, and the application demanded heat pipes in excess of 1 m in length. Because of these constraints, legacy knowledge of welding heat pipe end caps and fill tubes needs to be translated to the joining of 3D-printed multisection heat pipe constructions.

Historically, NASA and its engineering contractors have extensive experience in the design and testing of heat pipes. A comprehensive heat pipe manufacturing study was conducted in 1974 at the request of NASA Goddard Space Flight Center by F. Edelstein of the Grumman Aerospace Corporation (Ref. 4). Although production of refractory alloy-liquid metal heat pipes was not discussed, effective procedures for cheaper and more reliable heat pipe manufacturing methods were examined. Specifically, joint designs for welded caps and the effect of different welding processes on weld metallurgy, cost, and inspection were analyzed. A stepped (lipped) butt joint design was selected for recommendation because of its ease of alignment, ease of inspection, convenience when using filler material, and ability to produce consistent weld quality. This recommended stepped butt joint design can readily be drafted into CAD models exported to metal 3D printing systems.

Also documented in the 1974 report: heat pipe end closure was shown to be a problem with common concerns being porosity or cracks in the weld which can lead to a loss of the working fluid (Ref. 5). The remarks suggested parts should be joined with the fewest welds possible because welding heat adversely affects the mechanical properties of the material in the fusion zone (FZ) and heat affected zones (HAZs). The cast structure of the weld resulted in lower strength than that of the parent material and a reduced joint strength efficiency. To mitigate this issue, electron beam welding (EBW) can be used to create the narrowest weld and HAZ using high energy density with minimal heat input and distortion.

A two-volume heat pipe design handbook was commissioned by NASA Goddard Research Center and completed by P. J. Brennan and E. J. Krolczek of B&K Engineering in 1979 (Ref. 5). Within Volume I, allowable stresses for welded tubing were discussed. ASME code specifies that welding on heat pipes shall be performed on both sides (double-welded, inside and outside) and fully radiographed; however, single-welded joints are acceptable on thin-walled small diameter tubing as double-welding is impractical. The handbook also provided heat pipe life test data showing that with proper welding techniques, niobium (Nb-1Zr)-sodium heat pipes have survived 1,000 hr at 1,000 °C and over 16,000 hr at 850 °C; and niobium (Nb-1Zr)-lithium heat pipes surviving 9,000 hr at temperatures up to 1,500 °C.

In a 1981 report prepared for NASA Jet Propulsion Laboratory by D. M. Ernst of Thermacore Inc., refractory alloy liquid metal heat pipes were fabricated to assess complex geometries, bends, pipe transitions, and arterial wicks for service in power conversion subsystems within nuclear electric propulsion (NEP) spacecraft (Ref. 6). The work aimed to design a sodium or potassium heat pipe operating at 900 K with an internal pressure near 4 psi. Nb-1Zr was determined to be an acceptable material with sufficient creep strength for the application. Important conclusions stated heat pipe-to-heat pipe joints should be kept to a minimum within the constraints of system reliability and heat pipe-to-heat pipe joints should be integrally built if the system design permits.

Lessons learned from molybdenum-based heat pipes are also critical for the development of new AM-based refractory alloy heat pipes. A study by C. C. Silverstein of CCS Associates delivered to NASA Langley Research Center in 1986 investigated liquid metal heat pipe cooling systems for combustor liners and engine inlet leading edges of scramjet engines for missile applications (Ref. 7). Molybdenum-lithium heat pipes constructed from Mo alloy TZM operated up to 2600 °F and used carbon-carbon liners to extend the useful temperature range to 3400 °F. Molybdenum-lithium heat pipes were also discussed by B. L. Boman et al. in a 1989 NASA Langley Research Center contracted report for

hypersonic vehicle wing leading edge applications (Ref. 8). Molybdenum-based refractory alloy heat pipes offered easier integration into leading edges because their higher temperature capability has better performance with shorter lengths and reduced wick complexity. The fabrication and testing of Mo-Re heat pipes embedded in carbon-carbon was also conducted by D. E. Glass et al. for NASA Langley Research Center in 1998 (Ref. 9). A 3-ft-long Mo-Re-lithium heat pipe with a D-shaped cross-section was tested at an operating temperature of 2460 °F. The internal heat pipe vapor pressure measured at 2460 and 2820 °F was 16 and 52 psi, respectively. These reported internal pressures at various operating temperatures can serve as metrics to test heat pipes fabricated using AM.

Extremely relevant to the current research: a large effort on refractory alloy heat pipe accelerated life testing was carried out in the early 2010s by J. Martin et al. of NASA Marshall Space Flight Center (Ref. 10). A portion of the work focused on development of general welding procedures and wick manufacturing for Mo-44Re heat pipes. Three circumferential welds were performed during heat pipe closeout using EBW. There was concern regarding the critical single weld pass used to cap the severed heat pipe fill stem. Once welded, the Mo material can have a significantly reduced ductility due to interstitial impurities concentrated at the grain boundaries and a large, recrystallized grain structure. EB weld evaluation consisted of bend testing a series of welds made with varying process parameters to determine the weld’s effect on the material’s ductile-to-brittle transition temperature (DBTT). Typical EBW parameters found in literature for Mo-44Re used an accelerating voltage of 50 kV, primary beam current of 50 mA, and a welding speed of 30 mm/s. The same concerns of Mo-based wrought material are applicable to Nb-based printed material.

Presently, the fabricability of AM niobium alloy heat pipes needs further investigation to understand the weldability of printed niobium metal, the impact of producing a single heat pipe component with multiple joined sections on working fluid flow and capillary forces, and the eventual thermal performance of the niobium liquid metal heat pipe. In this work, flat and cylindrical (tubular) niobium heat pipe specimens were printed using the L-PBF process and welded together using EBW. A bead-on-plate study informed the EBW parameters. Inspection of the welds was conducted using optical metallography and computed tomography (CT). Additional aspects of heat pipe performance such as capillary flow of working fluid past welded joints and leak-tightness were determined.

2.0 Materials and Procedures

2.1 Niobium Alloy Powder Feedstock

The niobium alloy used throughout this work is C-103. The C-103 powder physiochemical information is provided in Table 1 and scanning electron microscopy (SEM) images of the powder are shown in Figure 1. D10, D50, and D90 refer to the particle diameters in which 10, 50, and 90 percent of particles are smaller. Note that while the Hf content within C-103 increases the Nb alloy weldability, Hf

TABLE 1.—NB ALLOY (C-103) POWDER
PHYSIOCHEMICAL PROPERTIES

Nb	Hf, wt%	Ti, wt%	Ta, wt%	W, wt%	C, wt%	O, wt%	D10, μm	D50, μm	D90, μm	Density, g/cm ³	Hall flow, sec/50
Bal.	9.6	1.0	0.2	0.2	0.005	0.029	15.4	28.6	49.5	8.83	11

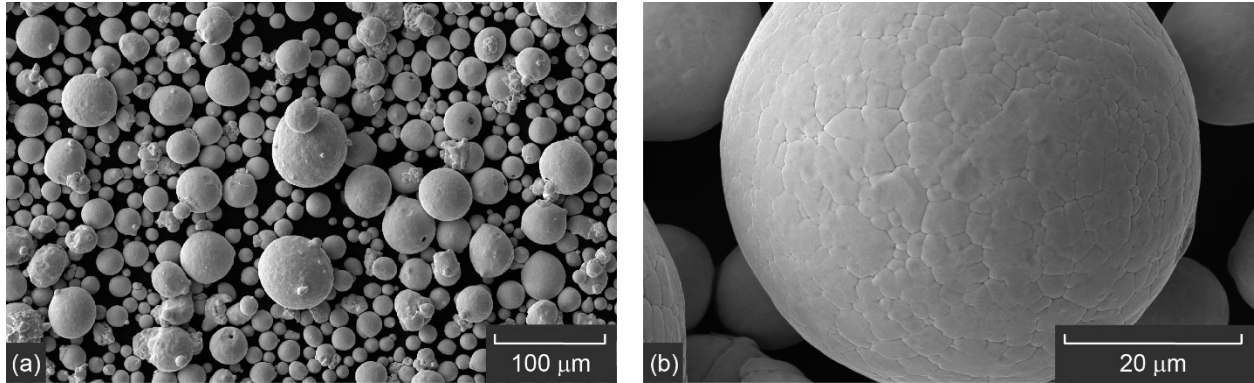


Figure 1.—Nb alloy (C-103) powder SEM SE images at 1 kx (a) and 8 kx (b) magnification.

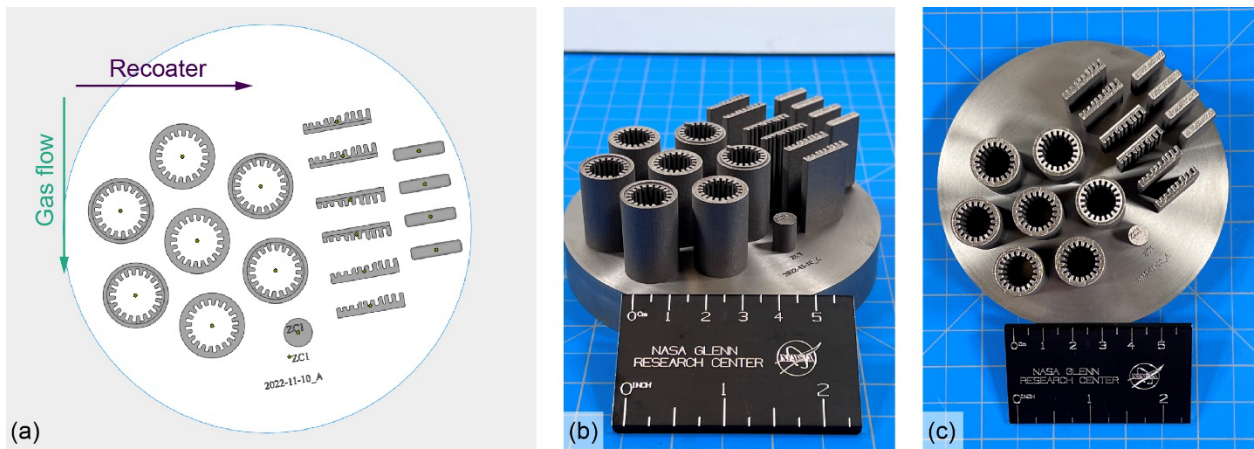


Figure 2.—Arrangement of printed specimens (a), build plate corner view image (b), and build plate top view image (c).

is not suitable in reactors because it increases the neutron cross section of niobium. Suitable replacement alloys exist but will need thorough print optimization before heat pipes can be manufactured to serve in such applications.

2.2 Laser Powder Bed Fusion

The L-PBF metal additive manufacturing process was performed in an EOS M100 machine using the parameters optimized to achieve 99.9 percent relative density. The build did not have contouring or changes in parameters for up-skin and down-skin conditions and was conducted in an Argon purged inert environment (<0.1% O₂).

Both flat and cylindrical heat pipe mock-up specimens were printed and arranged on a niobium build plate as shown in Figure 2. Following printing, the specimens were removed from the build plate via wire-EDM machining.

2.3 Heat Pipe Specimen Design

The flat heat pipe specimens were designed to examine both EBW parameters in the flat position and the effect of groove sizing on printability and capillary performance. Each flat specimen includes nine different grooves with widths of 0.5, 0.75, and 1.0 mm and heights of 1.0, 1.5, and 2.0 mm. A dimensioned image of the flat specimen is shown in Figure 3. Volume I of the 1979 heat pipe design handbook contains formulae for the sizing of axially grooved wick structures (Ref. 5). However, the formulae assume a smooth surface that may not account for the as-printed surface roughness of the L-PBF process.

Flat specimens of three different geometries were printed to assess the EBW of both a butt joint with adjoining surfaces ground with 600 grit SiC paper and a stepped butt joint with mating surfaces in the as-printed condition. A schematic of the combined three-part assembly is depicted in Figure 4. The stepped butt joint was designed into the CAD geometry with step dimensions intentionally offset by 0.05 mm wider than the desired final geometry to account for oversized prints, which is typical of the L-PBF process due to the influence of laser spot size on the local melt pool width.

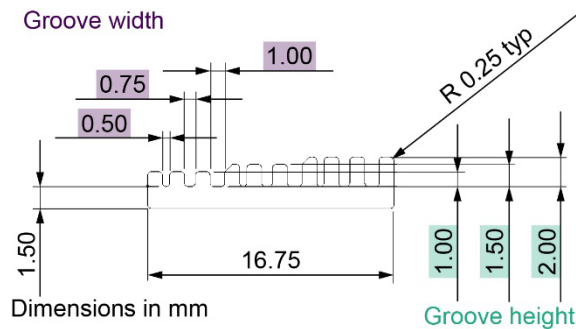


Figure 3.—Flat heat pipe specimen groove dimensions.

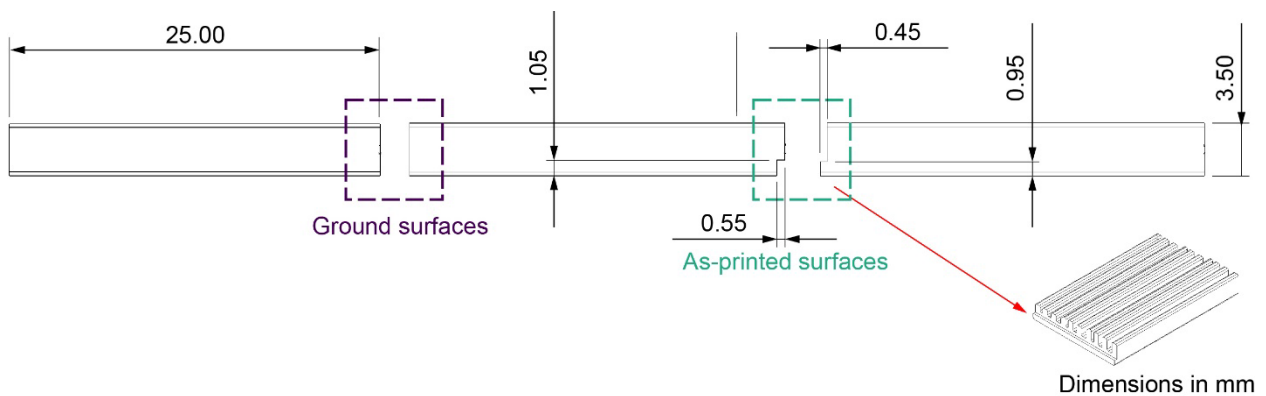


Figure 4.—Dimensioned schematic of the flat heat pipe mockup three-part assembly with the ground butt joint (a) and as-printed stepped butt joint (b).

The cylindrical heat pipe specimens were designed to examine both EBW parameters in the flat (1G) rotated position and the welds' ability to create a hermetic seal during leak testing. The internal grooves in the cylindrical specimens were fixed with a cross-sectional width of 1 mm and a height of 1.5 mm. The cylindrical specimens were tested in two different combinations: the first combination is a three-part assembly designed to examine the influence of mating surface finish on EBW butt joints, while the second is a two-part assembly with mating surfaces that have printed, engineered geometries with alignment features. The engineered male and female geometries include both a stepped butt for concentric alignment of the pipes and a locating-pin for alignment of the grooves. A schematic of the first combination is shown in Figure 5 and a schematic of the second combination alongside images of the engineered mating surfaces are shown in Figure 6.

The surface roughness of the ground and as-printed mating surfaces was measured using optical metrology on a Zygo Nexview™ NX2 3D Optical Profiler. The arithmetic average of the 3D roughness (S_a), root quadratic or root mean square average of the 3D roughness (S_q), and the maximum peak to valley height of the 3D roughness map (S_z) are listed in Table 2. Figure 7 provides 2D and 3D plots of the ground (a, b) and as-printed (c, d) surface roughness.

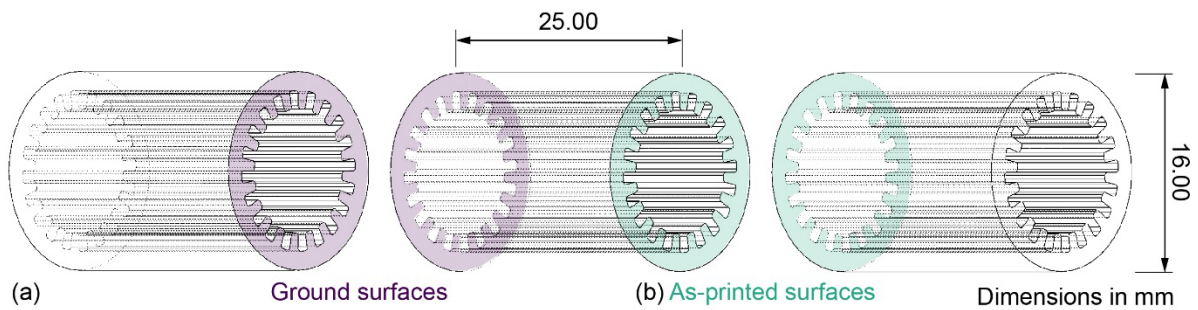


Figure 5.—Schematic of the cylindrical heat pipe mockup three-part assembly (Combination 1) with the ground butt joint (a) and as-printed butt joint (b).

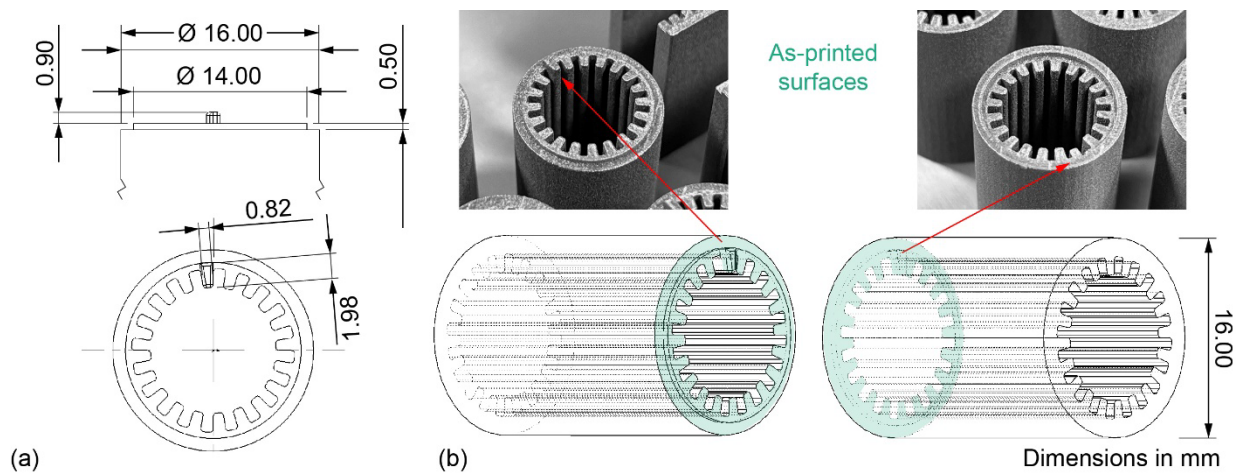


Figure 6.—Dimensioned schematic of the cylindrical heat pipe mockup two-part assembly (Combination 2) with the as-printed engineered step butt joint with male (a) and female (b) mating surfaces.

TABLE 2.—OPTICAL METROLOGY MEASUREMENTS OF THE GROUND AND AS-PRINTED MATING SURFACES

Mating surface	S_a , μm	S_q , μm	S_z , μm
Ground	0.203	0.265	4.904
As-printed	4.541	6.403	70.681

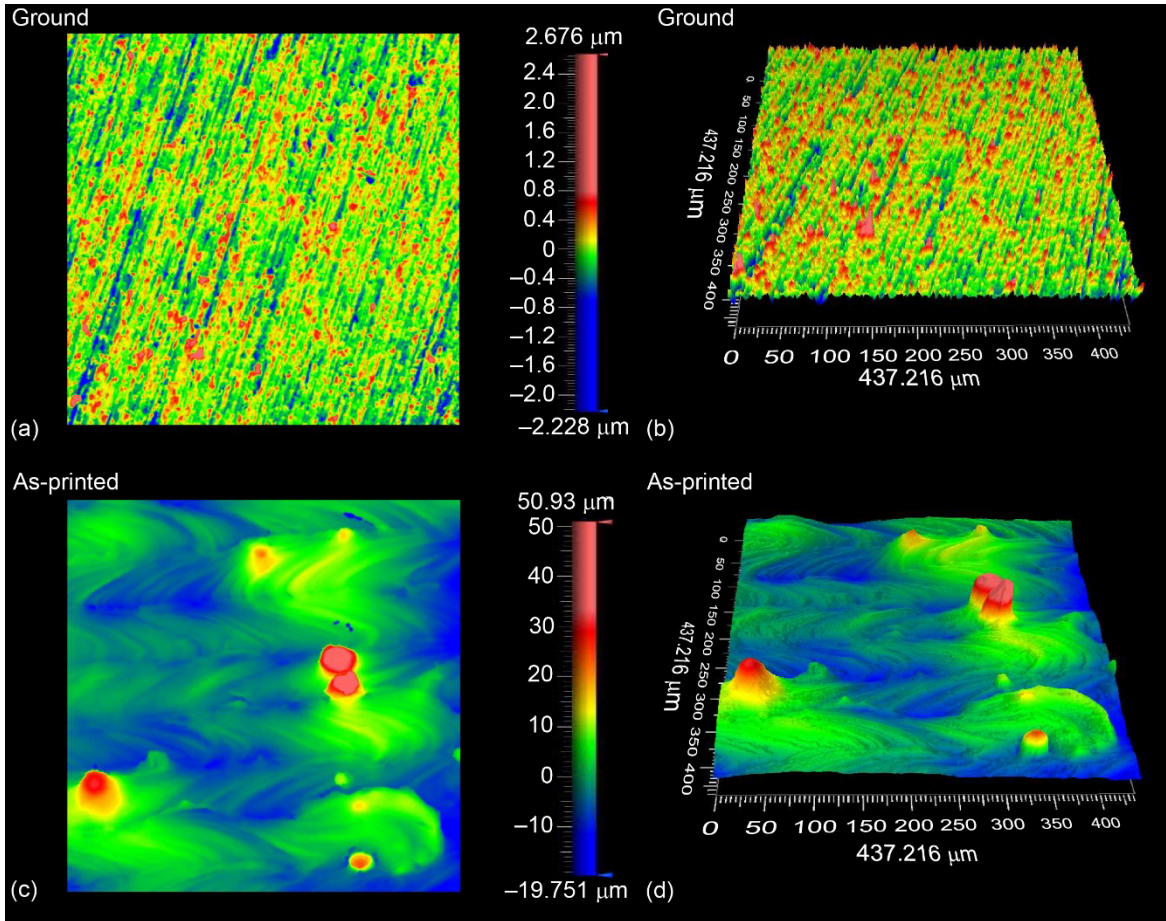


Figure 7.—2D and 3D plots of the ground (a, b) and as-printed (c, d) mating surfaces.

2.4 EBW Parameter Optimization

Prior to joining the flat and cylindrical heat pipe specimens, bead-on-plate EBW was conducted on a rectangular bar of wrought Nb-alloy with dimensions 155 by 27 by 13 mm. This EBW optimization was designed to determine parameters to achieve a defect-free weld with a 1 mm penetration depth. Before welding, the bar stock surface was prepared in accordance with the AWS C7.1 standard (Ref. 11). Eight welds were made using a constant voltage of 60 kV, currents ranging from 10 to 20 mA, and travel speeds ranging from 8.5 to 21.2 mm/s. Initial parameters were taken from AWS C7.1 Example 4 (Ref. 11). The welds were cross-sectioned, ground with SiC paper, polished using diamond suspensions to a 1 μm finish, and etched using one-part HF, one-part HNO_3 , and swabbed for 3 s. Optical micrographs were used to measure penetration depth and bead width using the open-source image analysis software ImageJ. A macro image of the bead-on-plate bar stock specimen alongside optical micrographs of the welds are shown in Figure 8. Bead width and penetration depth data for each of the eight welds is provided in Table 3.

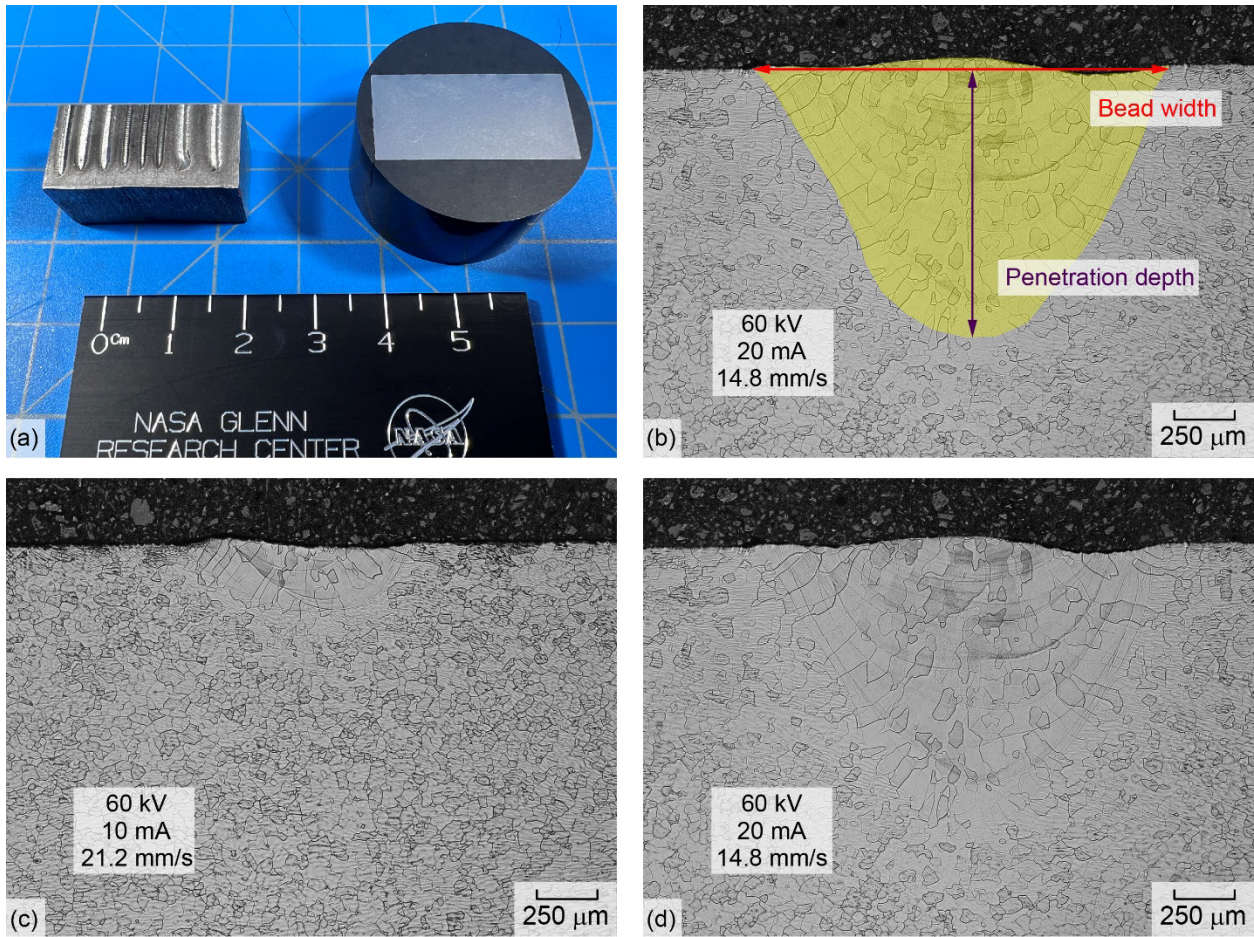


Figure 8.—Nb-alloy bead-on-plate EBW parameter optimization specimen (a), example of bead with and penetration depth measurements taken from the optical micrographs (b), EB weld with low current and high travel speed exhibiting low penetration depth (c), EB weld with high current and low travel speed exhibiting high penetration depth (d).

TABLE 3.—BEAD-ON-PLATE EBW PARAMETER OPTIMIZATION

Weld ID	Current, mA	Travel speed, mm/s	Bead width, mm	Penetration depth, mm
1	20	14.8	1.533	1.127
2	20	21.2	1.406	0.975
3	10	8.5	0.962	0.352
4	10	14.8	0.896	0.322
5	10	21.2	0.896	0.280
6	15	14.8	1.279	0.689
7	15	8.5	1.336	0.794
8	15	21.2	1.203	0.635

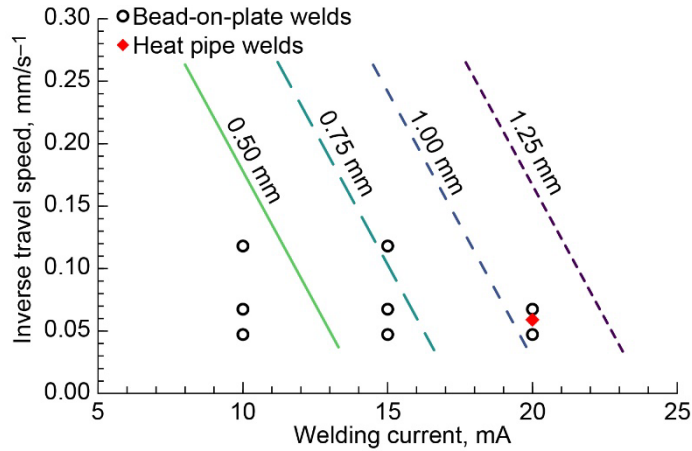


Figure 9.—60 kV EBW parameter curves to obtain 0.50 to 1.25 mm penetration depths.

From the eight EBW parameter optimization welds, penetration depth, d_p [mm], was determined as a function of beam current, I [mA], and travel speed, S [mm/s], using multiple linear regression (Equation 1). The regression analysis reported an R-Square value of 0.986 and an F-Significance of $2.22 \times 10^{-0.5}$.

$$d_p = 0.077 \cdot I + \frac{1.804}{S} - 0.591 \quad (1)$$

From Equation (1), EBW parameters can be determined to achieve a desired penetration depth. A graphical representation of Equation (1) is shown in Figure 9. From this optimization study, the parameters used to join both the flat and cylindrical heat pipe mock-ups were: 60 kV accelerating voltage, 20 mA beam current, and 16.9 mm/s travel speed (shown as the red diamond in Figure 9).

2.5 Flat Heat Pipe Capillary Performance Test and Metallography

Following welding of the flat heat pipe specimens, capillary performance testing examined both the ability of a working fluid to traverse a gap between two adjoining heat pipe sections and the effect of groove height and width on fluid wicking. The capillary performance test consisted of submerging an end of the welded flat heat pipe mock-up in an ethanol working fluid simulant. Video was captured at 240 frames per second to record position of the working fluid in the grooves. Still frames from the video were analyzed in ImageJ to determine wicking distance as a function of time. The ethanol was dyed red to increase visibility during image analysis. Capillary testing was performed at specimen inclinations of 30° and 90° with respect to the surface of the working fluid. An image of the 90° test set-up is shown in Figure 10.

Metallography of the flat heat pipe specimen consisted of optical imaging of the weld top surface and cross-section. Cross-sectioned welds were prepared for metallography using the method described in Section 2.4. Optical micrographs were used to measure penetration depth, bead width, and weld-centerline to joint misalignment.

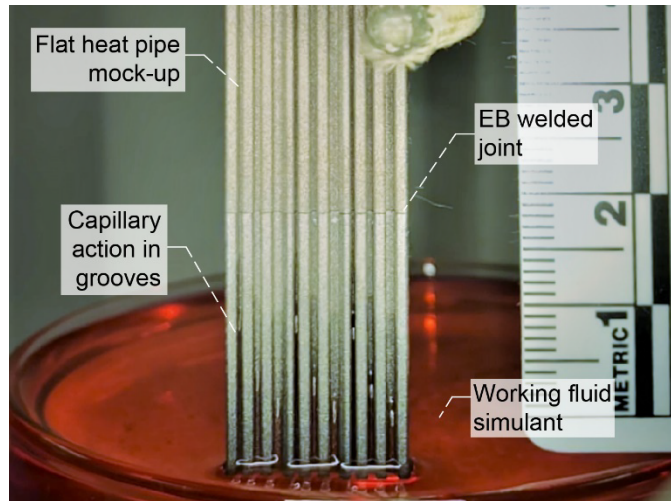


Figure 10.—Flat heat pipe mock-up capillary performance test set-up.

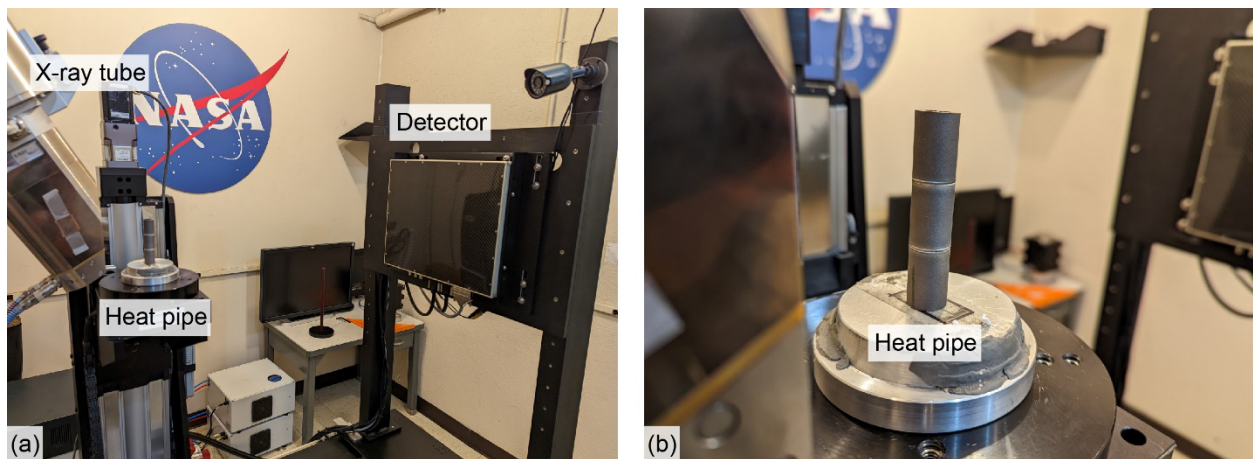


Figure 11.—Cylindrical heat pipe mock-up computed tomography test set-up.

2.6 Cylindrical Heat Pipe CT, Leak Test, and Metallography

The welded cylindrical heat pipe mock-up specimens underwent CT scanning to assess part fit-up and quantify weld defects like porosity. The CT scan used an Xray source voltage of 200 kV, current of 180 μ A, source-to-detector distance of 768 mm, part to detector distance of 688 mm, and magnification of 9.66X to achieve an optimum voxel size of 7.8 μ m. CT slice data was imported into ImageJ for 3D image analysis. The CT test set-up is shown in Figure 11.

Container design verification tests to confirm pressure containment integrity and leak tightness are detailed in Section 8.3 of the Heat Pipe Design Handbook Volume I (Ref. 5). To determine if the printed material was crack-free and the welds produced a hermetic seal, leak testing was conducted. A simple fixture was fabricated to hold the three-part mock-up assembly under water and pressurize the pipe with high-purity helium gas. Video was employed to capture any bubbling that might have occurred as pressure was increased using a regulator from 0 to 50 psi in 10 psi increments. The helium leak test fixture and test set-up are shown in Figure 12. Metallography of the cylindrical heat pipe specimen cross-sections were consistent with the methods used for the flat heat pipe specimens described in Section 2.5.

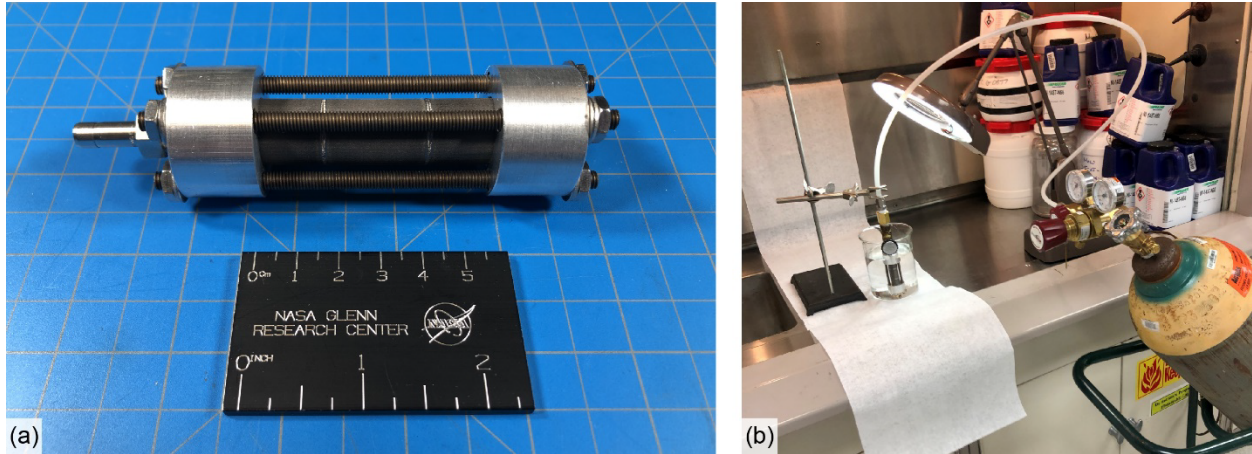


Figure 12.—Printed heat pipe leak test fixture (a) and helium leak test set-up (b).

3.0 Results and Discussion

3.1 Flat Heat Pipe Metallography

The ground and as-printed weld surface cross-sectional micrographs in Figure 13 show consistent weld penetrations of 1.199 and 1.253 mm, respectively. This consistency illustrates that the surface roughness of the mating surfaces had little impact on weld shape. Furthermore, both joints exhibited a uniform elliptical weld pool seen by the regular arc radii and melt pool cooling spacing.

With reference to the surface images in Figure 13(a) and (c), the weld of the ground mating surface (Figure 13(a)) had more irregularities observed as darkened regions where (during the sample cleaning process post-weld) ethanol stains emerged. This solvent staining may be occurring due to pores connected to the surface retaining ethanol after the drying step. This finding is consistent with porosity observed in the ground mating surface weld's cross-sectional metallograph (Figure 13(b)).

In Figure 13(b), a pore can be seen in the upper left corner of the weld pool. This pore formed during a keyhole instability where vaporized gas of the base material beneath the electron beam becomes trapped as a vapor bubble beneath the liquid melt pool. Subsequently these vapor bubbles attempt to rise to the surface of the melt pool but can be trapped given the fast electron beam travel speed and rapid solidification of the material. Interestingly, the metallograph of the as-printed mating surface (Figure 13(d)) does not show evidence of porosity. It is postulated that a larger gap at the leading edge of the weld pool due to increased surface roughness of the as-printed surfaces, creates an alternate avenue for gas to escape leading to less weld porosity.

Weld bead width and penetration depth data is provided in Table 4. The weld cross-sections in Figure 13(b) and (d) were also used to evaluate the amount of misalignment between the weld centerline and the joint. Although misalignment is primarily attributed to the placement and fixturing of the part in the EBW chamber, its magnitude can provide insight into melt pool behavior. The ground butt-joint had twice the misalignment of the as-printed step joint.

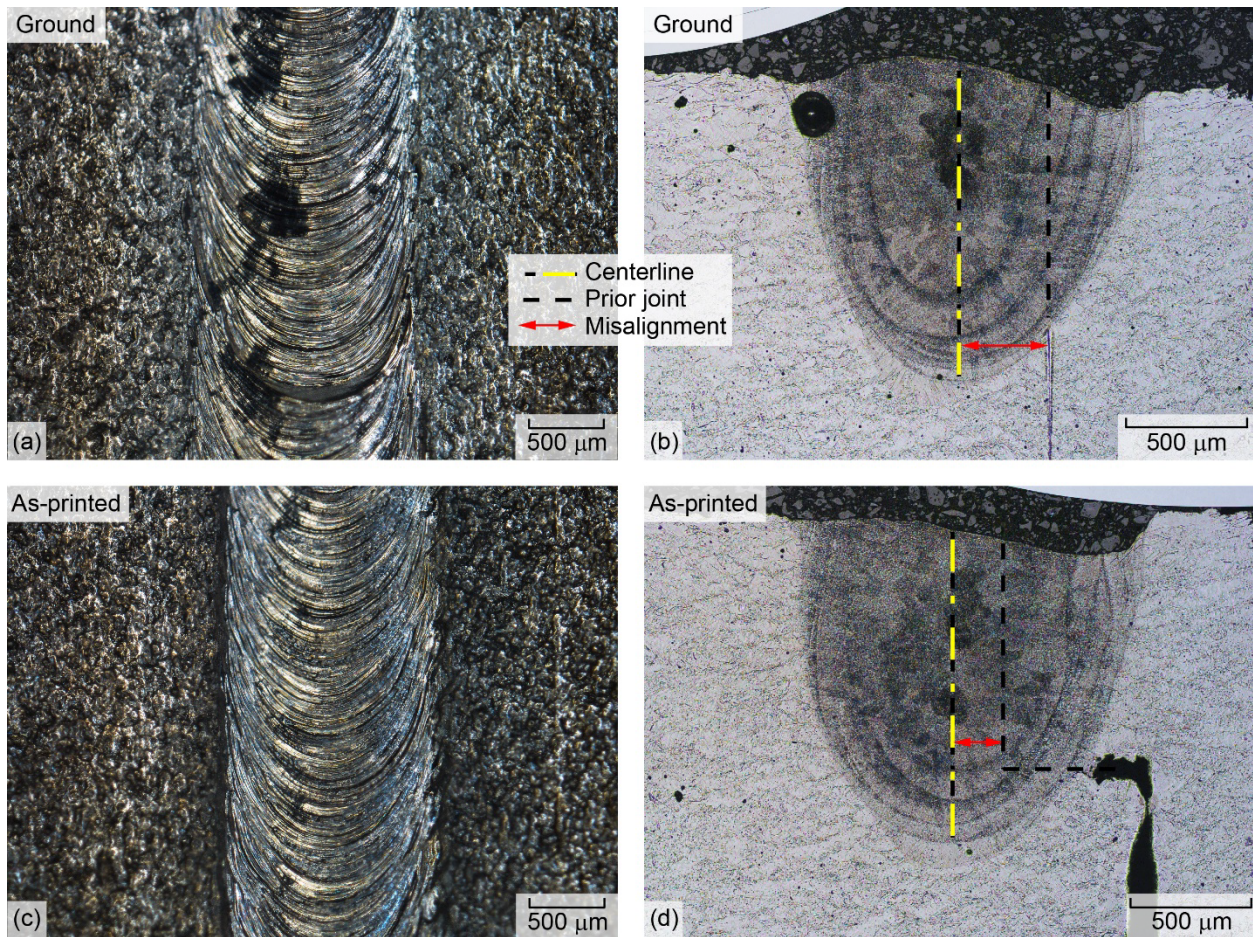


Figure 13.—Optical micrographs of the ground butt joint bead surface (a) and weld cross-section (b), and as-printed step joint bead surface (c) and weld cross-section (d).

TABLE 4.—FLAT HEAT PIPE MOCKUP SPECIMEN
IMAGE ANALYSIS DATA

Mating surface	Bead width, mm	Penetration depth, mm	Misalignment, μm
Ground	1.323	1.199	376.4
As-printed	1.257	1.253	124.4

3.2 Flat Heat Pipe Capillary Performance Testing

Wicking distance versus time was plotted for both the 90° and 30° inclination capillary performance tests in Figure 14. The capillary force of the ethanol working fluid simulant was not great enough to permit wicking past the EB weld located approximately 25 mm from the end of the flat heat pipe specimen during the 90° inclination test. However, during the 30° test, all three of the grooves with a width of 0.5 mm (shown in the purple color in Figure 14(b)) were able to quickly climb and easily wick past the EB joint. This test proved that, provided proper alignment of the grooved wick structure is maintained during welding, adequate capillary force can be achieved. Overall, the EB weld does not provide significant resistance to the flow of the heat pipe working fluid. From this examination, it is expected that future heat pipe design using L-PBF pipe section can include joined sections without limiting capillary performance.

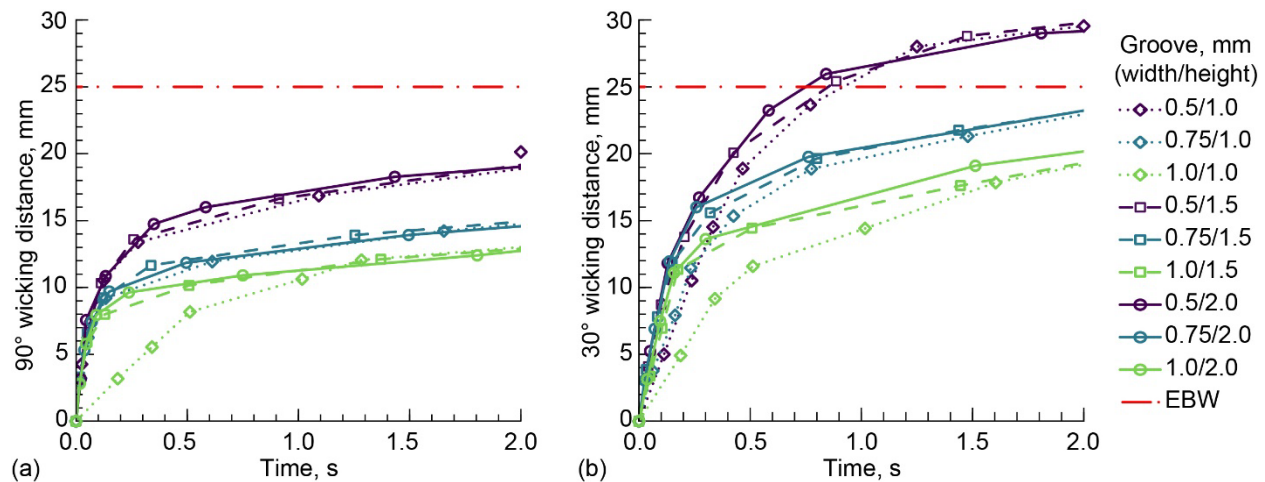


Figure 14.—90° (a) and 30° (b) inclination capillary performance test of grooved flat heat pipe specimen.

As anticipated, the heat pipe groove shape affected fluid wicking performance. The width of the groove has a much larger impact on wicking distance compared to groove height. Based on the wicking distance versus time data in Figure 14, the smallest tested groove width of 0.5 mm exhibited the greatest wicking distance of 30 mm (nearly two times farther than the 1.0 mm groove width). Less discernable is the trend between groove height and capillary performance. Overall, the tallest groove height of 2.0 mm achieved the fastest wicking rates. This can be attributed to the increased surface area of the groove compared to the shorter groove heights examined. Within this study, total optimization of groove design was not a priority. Further examination of heat pipe wick structure is needed before final design review. There is ongoing research studying the ability to print porous-type integrated wick structures using the L-PBF process.

3.3 Cylindrical Heat Pipe Computed Tomography

A single slice for the ground and as-printed mating surface welds are shown in Figure 15(a) and (c), respectively. Note that refractory metals including niobium have high radio-opacity, meaning that often insufficient x-ray flux penetrates the part to reach the detector. However, the thin-wall pipe geometry used in this work is amenable to the CT scanning process for refractories and was able to provide images with acceptable contrast and resolution. Weld porosity was immediately observable in the CT images. A grouping of CT slices encompassing the whole weld were sectioned and thresholded as an image stack in ImageJ to measure the number of observable weld indications (pores), the total volume of porosity, and average pore diameter in both the ground and as-printed mating surface welds. The weld porosity data is provided in Table 5. The measured porosity is highlighted in red in the 3D representation of the weld section of the ground and as-printed mating surface specimens (Figure 15(b) and (d)). Contrary to expectations, the ground mating surface had an order of magnitude greater number of indications and volume of porosity than the as-printed surface. Both ground and as-printed surfaces had an average pore diameter around 50 to 60 μm . The porosity is not interconnected and is trapped near the middle of the weld through thickness; as such, the porosity is not expected to create a path for leaks. However, the absence of weld material will negatively impact the strength of the joint.

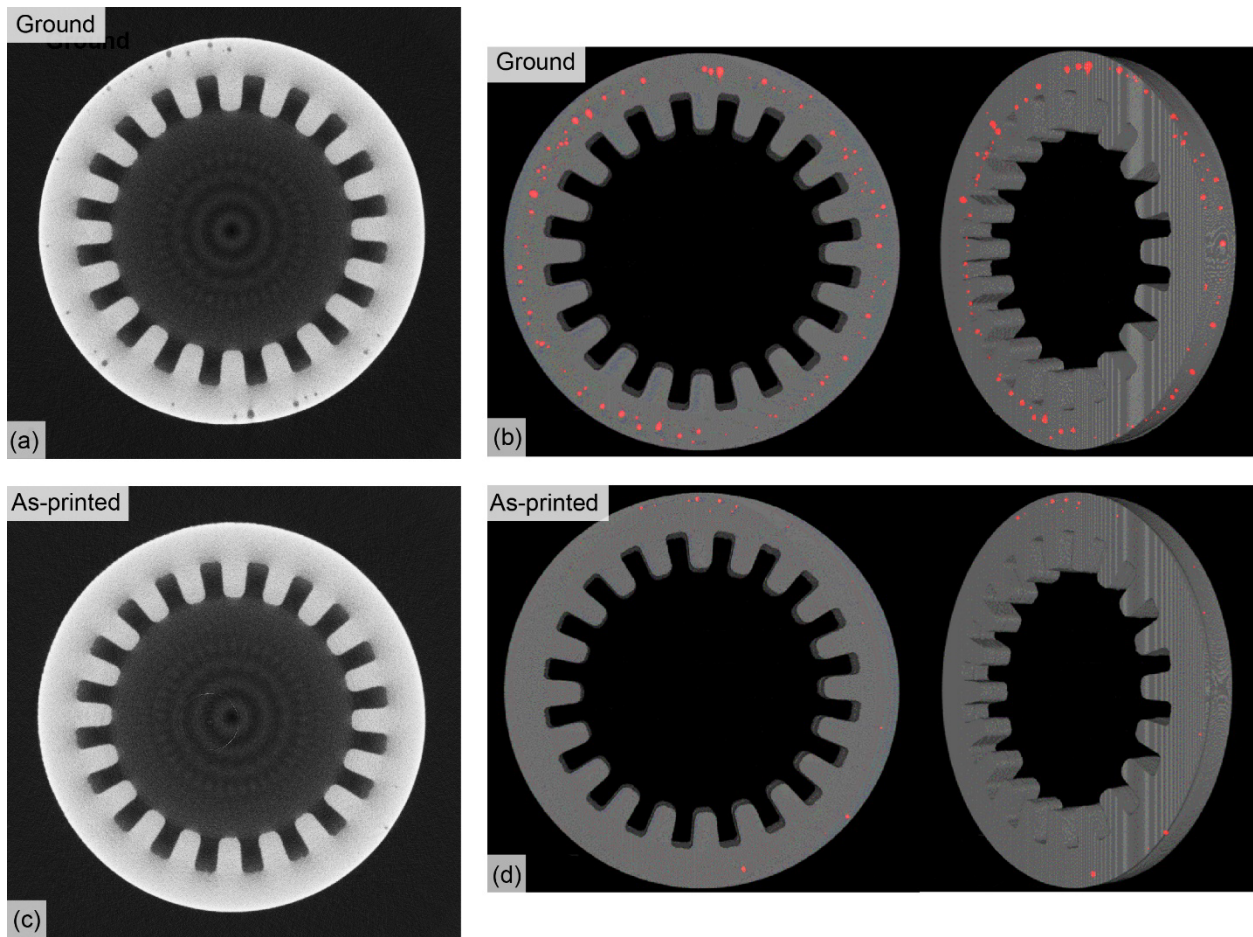


Figure 15.—CT slice and translucent 3D rendering highlighting weld porosity (red) of the ground (a, b) and as-printed (c, d) cylindrical heat pipe butt joints.

TABLE 5.—WELD POROSITY DATA FROM CT IMAGING

Mating surface	Indication count	Porosity volume, mm ³	Average pore diameter, μm
Ground	1261	0.16456	62.9
As-printed	132	0.00919	51.0

The ability of the alignment pin on the engineered heat pipe specimen to orient the grooves of the heat pipe was examined using the CT data. When the ground butt mating surface was tacked together, the grooves were aligned by eye which can introduce error during fabrication. The pin and recess designed into the engineering specimen aimed to ease the alignment process in the tacking procedure. The CT data's 3D reconstruction of the ground butt joint is shown in Figure 16(a) and exhibits a groove misalignment of 0.53°. Similarly, the engineered as-printed joint is shown reconstructed in Figure 16(b) to (d). Although the engineered joint had a greater degree of misalignment of 1.32°, anecdotal description of the tacking process from the welding technician stated the alignment pins saved time and effort. CAD to enhance part fit-up and alignment will be conducted in a future investigation.

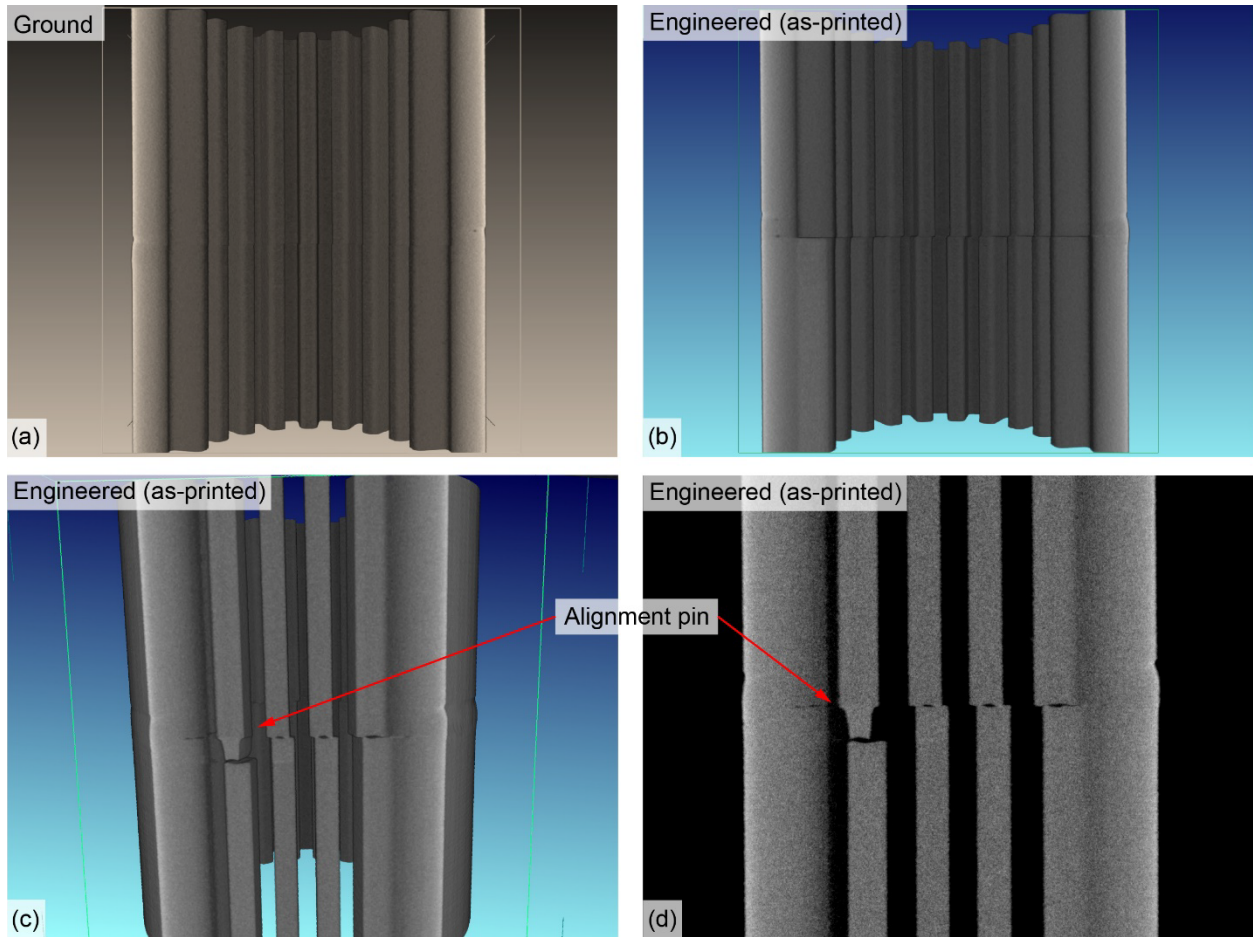


Figure 16.—CT 3D reconstructions of the ground mating surface joint (a), engineered mating surface joint (b), and the engineered mating surface joint highlighting the alignment pin (c); CT slice of the engineered joint showing the alignment pin (d).

3.4 Cylindrical Heat Pipe Leak Testing and Metallography

As high temperature niobium heat pipes may experience an internal pressure greater than 50 psi during operation, it is critical that the printed material and welds create a hermetic seal. The three-part cylindrical heat pipe specimen was placed into the leak test fixture and submerged in water. Gaseous helium was used to pressurize the pipe from atmosphere to an internal pressure of 50 psi in increments of 10 psi. No bubbling or leaks were observed. Following pressurization to 50 psi, the cylinder was isolated from the pressurized gas cylinder and held at a constant pressure for 1 hr. The cylinder remained at 50 psi for the entire hour duration (Figure 17). Although 50 psi may not be the maximum internal pressures expected during service, the leak test proved that there are no interconnected cracks or porosity networks within the bulk printed C-103 or welds.

Following leak testing, the welds were cross-sectioned for metallography. The ground and as-printed mating surface weld cross-sections are shown in Figure 18. Both welds achieved the desired 1 mm penetration depth.

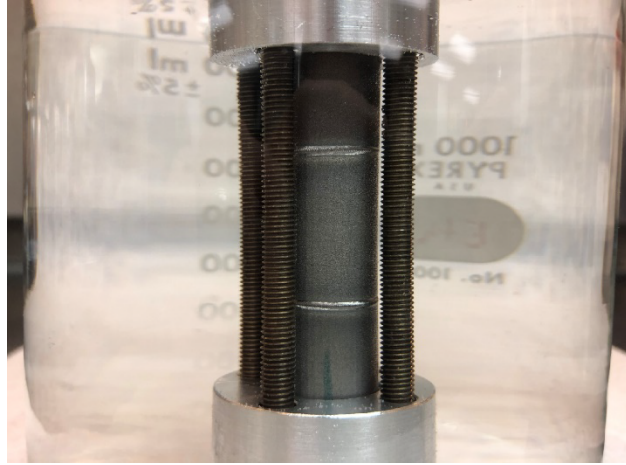


Figure 17.—Leak test of EB welded three-part cylindrical heat pipe specimen pressurized to 50 psi.

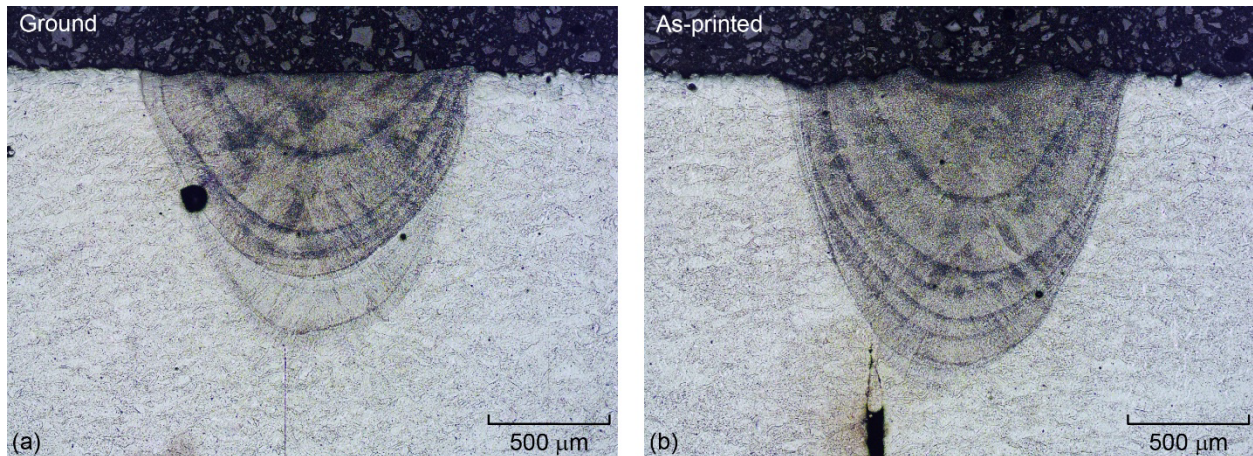


Figure 18.—Optical micrographs of the ground butt weld cross-section (a), and the as-printed butt joint weld cross-section (b).

3.5 On the Fabricability and Future Study of 3D Printed Niobium Heat Pipes

The fabricability of high-temperature niobium alloy heat pipes using modern L-PBF metal additive manufacturing and existing EBW technologies is excellent and readily achievable. Eliminating the traditional subtractive methods helps reduce material costs and fabrication lead times. The ability to design locating and alignment features into the heat pipes takes advantage of the unique capabilities of additive manufacturing. This EBW study aimed to quell concerns with joining multiple sections of printed heat pipes; specifically, the ability of the working fluid to wick past an EB welded joint, and the ability of the printed material and welds to produce a hermetic pipe container. Today’s largest L-PBF machines like the Velo3D Sapphire XC have chambers with maximum building heights nearing 1 m. Although these machines can produce the meter plus long heat pipes needed for envisioned space propulsion systems with two or three prints and on or two welds, it would require hundreds of kilograms of expensive refractory alloy spherical powder feedstock. A more practical and cost-effective approach involves printing more sections with a multitude of joints in a smaller chambered L-PBF machine.

A significant amount of porosity was observed in the EB welds of the flat and cylindrical heat pipe specimens, particularly in the joints with the ground mating surfaces. As mentioned in Section 1.0, porosity in the weld can lead to a loss of the working fluid (Ref. 5). Strategies for mitigating EBW porosity include reducing the weld travel speed to allow porosity time to escape or defocusing the beam to transition into the conduction welding mode instead of the keyhole regime. The reduced weld porosity volume of the rougher as-printed joints also comes with the added benefit of eliminating the sharp notch just below the weld root that can cause stress concentration.

Future high-temperature heat pipe studies will investigate the ability to create porous wicking structures by adapting L-PBF parameters to create a partially dense material or mesh. Optimization of wicking structures is currently being performed by many researchers as described in Reference 2. A similar study should be performed for refractory alloys to increase the integrated niobium wick's capillary force and therefore thermal performance of the heat pipes. Directly following this work, multiple niobium heat pipe sections will be printed using L-PBF, joined using EBW, and then filled with a sodium working fluid. Thermal performance testing of the grooved niobium heat pipes is to be conducted using induction heating and thermocouples.

4.0 Summary and Conclusions

Modern metal AM has revolutionized the manufacturability of refractory alloy high-temperature heat pipes. However, building of meter-plus length heat pipes necessitates the joining of multiple pipe sections due to build chamber height limitations within state-of-the-art metal 3D printing systems. In this work, EB welds conducted on Nb alloy C-103 printed using the L-PBF process were characterized via image analysis of optical micrographs and CT scans to assess differences in weld geometry and indications under various EB parameters and joint designs. EBW of heat pipe sections examined the joint's impact on working fluid wicking and pipe leak-tightness. From the study, the following conclusions can be drawn:

1. EB welded joints connecting multiple heat pipe sections do not impact working fluid wicking behavior. The working fluid simulant wicked rapidly past the EBW joint during a 30° incline capillary performance test.
2. The printed C-103 material and the EB welds joining the tubular sections created a leak-tight container that withstood a 50 psi pressurization of gaseous helium. The hermetic seal for encapsulation of the working fluid held pressure for an hour before the test was stopped.
3. CT data showed an order of magnitude greater number and volume of porosity indications in the ground mating surface weld (0.165 mm³) compared to the as-printed mating surface weld (0.009 mm³); which is contrary to expected EBW behavior. Porosity can be mitigated in future assessments by modifying EBW parameters to allow time for trapped gas to escape.
4. Integral wick structures, stepped joints for welding, and features for groove alignment were easily designed in the 3D-printed part geometry. Such features take advantage of the AM process and save time during heat pipe manufacturing.
5. Optimal niobium alloy EBW parameters to achieve a 1 mm penetration depth was determined (60 kV accelerating voltage, 20 mA beam current, and 16.9 mm/s travel speed and a characteristic equation was developed (Equation (1)) to adjust EBW parameters for joining of niobium heat pipes with varying wall thicknesses.

These findings demonstrate the feasibility of using EBW to join Nb alloy C-103 heat pipe sections printed using the L-PBF process. The results provide a foundation for further research on the use of AM to manufacture high-performance refractory alloy heat pipes.

References

1. M. Chaiken, M. Gibson, and J. Sanzi, "Heat Pipe Development for Space Fission Demonstration Missions," in *Nuclear and Emerging Technologies for Space*, 2021.
2. P. Szymanski and D. Mikielwicz, "Additive Manufacturing as a Solution to Challenges Associated with Heat Pipe Production," *Materials*, vol. 15, no. 4. MDPI, Feb. 01, 2022. doi: 10.3390/ma15041609.
3. D.H. Lee and I.C. Bang, "Additive manufacturing and charging procedure of high-temperature heat pipe for nuclear reactor application," in *Transactions of the Korean Nuclear Society Virtual Autumn Meeting*, Ulju-gun, Ulsan, 2021.
4. F. Edelstein, "NASA CR-139140 Heat Pipe Manufacturing Study," Greenbelt, Maryland, 1974.
5. P.J. Brennan and E.J. Kroliczek, "Heat Pipe Design Handbook - Volume I," Towson, Maryland, 1979.
6. D.M. Ernst, "NASA CR-164878 Heat Pipe Heat Rejection System and Demonstration Model for the Nuclear Electric Propulsion (NEP) Spacecraft," Pasadena, California, 1981.
7. C.C. Silverstein, "NASA CR-4036 Heat Pipe Cooling for Scramjet Engines," Bethel Park, Pennsylvania, 1986.
8. B.L. Boman, K.M. Citrin, E.C. Garner, and J.E. Stone, "NASA CR-181922 Heat Pipes for Wing Leading Edges of Hypersonic Vehicles," St. Louis, Missouri, 1990.
9. D.E. Glass, M.A. Merrigan, and J.T. Sena, "NASA CR-207642 Fabrication and Testing of Mo-Re Heat Pipes Embedded in Carbon/Carbon," Hampton, Virginia, 1998.
10. J. Martin, R. Reid, E. Stewart, R. Hickman, and O. Mireles, "Closeout Report for the Refractory Metal Accelerated Heat Pipe Life Test Activity," Huntsville, Alabama, 2013. [Online]. Available: <http://www.sti.nasa.gov>
11. American Welding Society, *AWS C7.1: Recommended practices for electron beam welding and allied processes*, 4th ed. 2013.

